Volume XXIX 2026
MBNA Publishing House Constanta 2026

Scientific Bulletin of Naval Academy

SBNA PAPER • OPEN ACCESS

Gas Turbine Propulsion Systems for Naval Vessels: Energy Flow Calculation Methodology and High-Pressure Rotor CFD Simulation

To cite this article: Volintiru Octavian-Narcis, Adrian Popa, Daniel Mărășescu, Doru Coșofreț and Scurtu Ionuț-Cristian, Scientific Bulletin of Naval Academy, Vol. XXIX 2026, pg. 61-72.

Submitted: 24.04.2026
Revised: 31.07.2026
Accepted: 04.08.2026

Available online at www.anmb.ro

ISSN: 2392-8956; ISSN-L: 1454-864X

doi: 10.21279/1454-864X-26-I1-006

Gas Turbine Propulsion Systems for Naval Vessels: Energy Flow Calculation Methodology and High-Pressure Rotor CFD Simulation

Volintiru Octavian-Narcis[1], Adrian Popa[1*], Daniel Mărășescu[1], Doru Coșofreț[1] and Scurtu Ionuț-Cristian[1]
[1]Naval Academy "Mircea cel Bătrân", Marine Engineering Faculty, Department of Naval Engineering Systems, octavian.volintiru@anmb.ro
*** adrian.popa@anmb.ro**

Abstract. This paper addresses the modernization of naval propulsion systems through the adoption of gas turbine technology, with emphasis on thermodynamic calculation methodology and rotor flow simulation. The study is centred on the Rolls Royce gas turbine, employed in naval propulsion applications and covers all thermodynamic states from atmospheric air intake through the two-stage compression process, combustion chamber, high-pressure and low-pressure turbine stages, to the power turbine exhaust. Key parameters, including mass flow rates, stage temperatures, pressure ratios, stage power outputs, and overall thermal efficiency (η = 0.337), are systematically derived using polytropic compression relations and energy balance equations. In the second part of the paper, a 3D model of the gas turbine high-pressure rotor is developed in SolidWorks and subjected to CFD flow simulation. Three rotational speed regimes are analysed, 500 rad/s, 750 rad/s, and 1000 rad/s, with corresponding inlet boundary conditions of temperature, pressure, and velocity. The simulation results reveal total pressure drops across the rotor of 1.1%, 1.64%, and 2.3% respectively, consistent with increasing energy extraction at higher rotational speeds. Convergence of total pressure at both rotor inlet and outlet confirms numerical stability across all cases. The results provide a quantitative basis for performance assessment and design optimisation of naval gas turbine rotors.
Keywords: gas turbine; energy flow; Rolls Royce; CFD simulation; rotor; thermodynamic efficiency.

1. Introduction

The continuous development of naval technology and the need to enhance the performance of modern military vessels have driven the adoption of increasingly efficient and adaptable propulsion systems. In this context, gas turbines have gained considerable importance in naval propulsion, owing to their high power-to-weight ratio, short start-up time, and operational flexibility across a wide speed range (Sui et al., 2020; Budiyanto et al., 2024). Combined propulsion systems — such as COGOG, COGAG, CODOG, and CODAG - exploit the complementary performance envelopes of gas turbines and diesel engines, enabling optimised fuel consumption across the full operational speed range while preserving tactical responsiveness (Ghose & Gokarn, 2004; Friedman, 2006).

The modernization of naval fleets represents a strategic priority for increasing operational readiness and maritime security. Propulsion systems are central to ensuring the mobility and autonomy of vessels, directly influencing their performance in combat, patrol, escort, and intervention missions. Among the platforms that stand to benefit from such modernization, frigates represent a class where propulsion efficiency, acoustic signature reduction, and maintainability are simultaneously critical requirements (Sahraoui et al., 2024). The T22-class frigate, originally fitted with a COGOG arrangement comprising

Rolls Royce Tyne cruise turbines and Rolls Royce Olympus boost turbines, represents a reference platform for evaluating propulsion modernisation strategies (Bălan, 2016).

Significant research has been conducted on the thermodynamic modelling and performance simulation of naval gas turbines. Campora (2024) developed a thermodynamic simulator for the WR21 intercooled recuperated gas turbine, demonstrating its applicability to ship propulsion studies under variable operating conditions. Fatsis (2022) investigated the enhancement of gas turbine performance through wave rotor technology, reporting measurable gains in thermal efficiency for naval applications. Coraddu et al. (2016) applied machine learning techniques to condition-based maintenance of naval propulsion plants, highlighting the value of high-fidelity simulation data as a training basis for predictive models. Ma et al. (2023) constructed a data-driven digital twin framework for gas turbine anomaly detection, further underlining the importance of accurate thermodynamic and flow characterisation. In the field of combined propulsion system matching, Bob-Manuel and Okim (2018) addressed the optimisation of CODOG arrangements for frigates, while Xu et al. (2018) analysed novel COGAG configurations for improved part-load efficiency. Ren et al. (2019) examined the influence of the Energy Efficiency Design Index on ship-engine-propeller matching, demonstrating the growing importance of thermodynamic optimisation in naval propulsion design.

Despite this body of work, detailed energy flow calculations covering all thermodynamic stations of a two-spool naval gas turbine - combined with CFD-based rotor simulation across multiple speed regimes - remain relatively scarce in the open literature, particularly for the Rolls Royce Tyne turbine family.

The purpose of this paper is twofold. First, to present a complete thermodynamic methodology for calculating energy flows at all key cycle stations of the Rolls Royce gas turbine, employed in naval propulsion, using polytropic compression relations and energy balance equations. Second, to develop a 3D model of the high-pressure turbine rotor in SolidWorks and perform CFD flow simulations at three rotational speed regimes - 500 rad/s, 750 rad/s, and 1000 rad/s - in order to characterise the pressure distribution and energy extraction behaviour across the rotor. The results provide a quantitative basis for performance assessment and design optimisation of naval gas turbine propulsion systems.

2. Materials and methods

This study combines analytical thermodynamic modelling with computer-aided 3D design and computational fluid dynamics simulation. The methodology follows two parallel tracks: the calculation of energy flows at all thermodynamic stations of the Rolls Royce gas turbine using classical cycle analysis, and the development of a parametric 3D rotor model and its subsequent CFD investigation under three rotational speed regimes. All numerical work was performed using commercially available engineering software, and the results were interpreted against published turbine performance data.

2.1. Case Study

The reference platform for this study is a T22-class frigate, a naval vessel originally equipped with a COGOG combined propulsion arrangement comprising Rolls Royce Tyne cruise turbines and Rolls Royce Olympus boost turbines. The propulsion shaft arrangement of the T22-class frigate is subject to torsional vibration constraints that influence the selection and sizing of the gearbox and coupling components, a consideration addressed in naval shaft design by Homišin et al. (2020). The Tyne turbine, a two-spool axial-flow gas generator with a single-stage free power turbine, serves as the subject of the thermodynamic analysis. Its rated effective power output is 4,000 kW, with a total compression ratio of 10.37:1 distributed across a 5-stage low-pressure compressor and a 7-stage high-pressure compressor. The maximum fuel flow rate is 1,000 kg/h of naval diesel fuel, with a net calorific value of 42,702 kJ/kg. The gas turbine installation layout, covering all key components and thermodynamic stations from atmospheric air intake to exhaust, is presented in Figure 2.

2.2. Materials

The thermodynamic cycle calculations were performed analytically, using the nominal and assumed parameters of the Rolls Royce Tyne turbine as tabulated in the original technical documentation (Bălan, 2016; Siemietkowski, 1970). The working fluid properties used throughout the calculation are: specific heat of air $c_a = 1.05$ kJ/(kg·K), specific heat of exhaust gas $c_g = 1.20$ kJ/(kg·K), and polytropic index $n_k = 1.395$. The air excess coefficient was taken as $\alpha = 1.64$, with a stoichiometric air-fuel ratio of $m_{at} = 14.4$ kg_{air}/kg_{fuel}. A uniform isentropic efficiency of $\eta = 0.82$ was applied to all compressor and turbine stages, consistent with values reported for gas turbines of this class in the literature (Niculescu et al., 2020). The fuel energy utilisation factor in the combustion chamber was $\xi = 0.523$. The fuel energy utilisation factor $\xi = 0.523$ represents the fraction of fuel chemical energy flux converted into useful thermal energy of the working gas at the combustion chamber outlet. This coefficient, defined following the methodology of Bălan (2016), accounts for combustion losses, wall heat losses, and incomplete energy transfer specific to the tubular combustion chamber configuration of the Tyne turbine, and is not equivalent to the combustion efficiency index used for modern annular combustors.

The 3D geometry of the high-pressure turbine rotor (Figure 1) was constructed using SolidWorks 2023, a parametric solid modelling environment widely used in mechanical and marine engineering design (Dassault Systèmes, 2023). The rotor assembly comprises nine individual components, including the rotor disc, blade carrier, twisted rotor blades, and exhaust casing. SolidWorks Flow Simulation, an integrated CFD module based on the finite volume method with automatic Cartesian mesh generation, was used to perform the flow analyses (Dassault Systèmes, 2023). The working fluid was modelled as an ideal gas with properties representative of high-temperature combustion products.

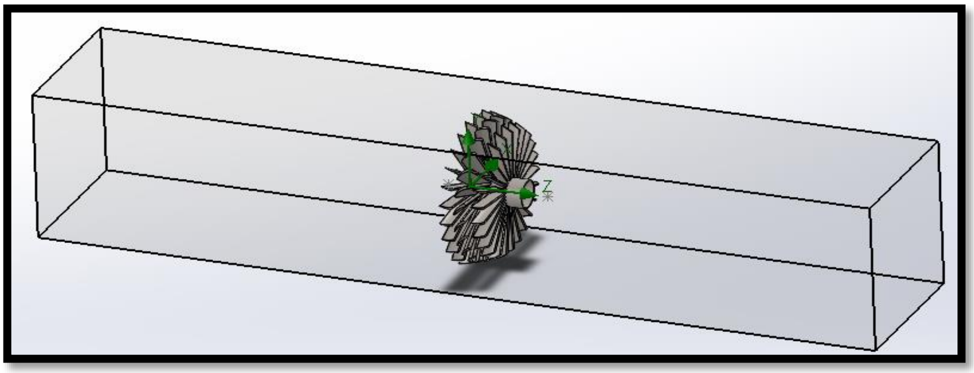

Figure 1. Rotor Geometry.

2.3. Methods

The thermodynamic analysis follows the classical open-cycle gas turbine methodology, applied station by station along the gas path (Campora, 2024; Fatsis, 2022). Eight reference stations are defined, from atmospheric air intake through low-pressure compression, high-pressure compression, combustion, high-pressure turbine expansion, low-pressure turbine expansion, power turbine expansion, and exhaust to atmosphere. At each compression stage, the outlet temperature is determined from the polytropic relation, where the stage pressure ratio and the polytropic index are the governing parameters. The energy flux imparted to the air by each compressor stage is computed from the air mass flow rate, the specific heat, and the temperature rise. In the combustion chamber, the total gas energy flux is the sum of the air enthalpy and the fraction of fuel energy utilised. For each turbine stage, the energy extracted by the gas is derived from the compressor work requirement, corrected for stage efficiencies, and the corresponding temperature drop is computed from the gas mass flow rate and specific heat. The overall thermal efficiency of the installation is evaluated from the ratio of effective shaft power to total fuel energy input, following the approach described by Campora (2024) and Fatsis (2022). The SolidWorks Flow Simulation framework, based on the finite volume method, was selected for its suitability to parametric rotor studies at this level of geometric fidelity. Recent advances in CFD simulation of gas turbine flows, reviewed by Zhu et al. (2021), confirm that finite-volume solvers provide reliable pressure and velocity field predictions for simplified rotor geometries, making them appropriate for the parametric analysis conducted in the paper.

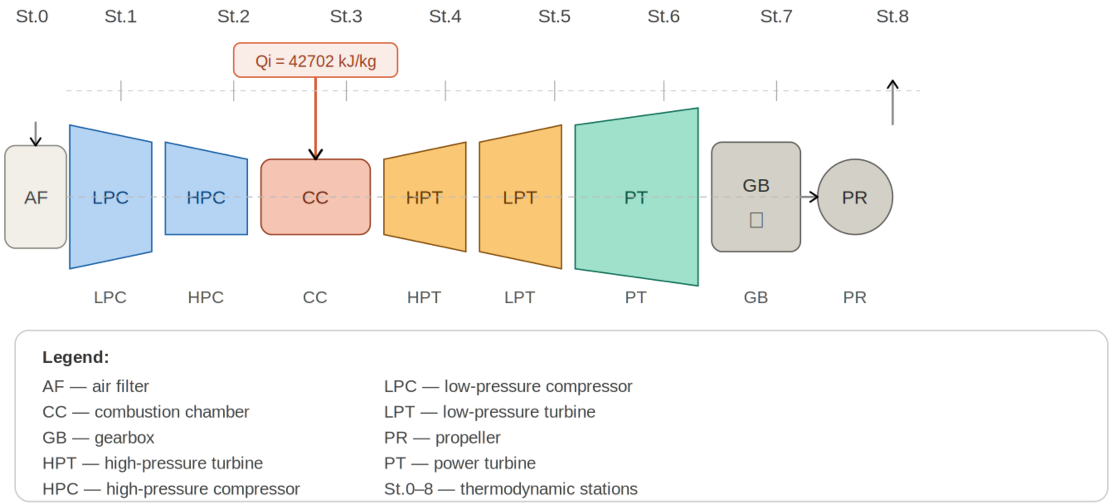

Figure 2. Schematic of the Rolls Royce Tyne gas turbine propulsion installation. AF - air filter; LPC - low-pressure compressor; HPC - high-pressure compressor; CC - combustion chamber; HPT — high-pressure turbine; LPT - low-pressure turbine; PT - power turbine; GB - gearbox; PR - propeller. St.0–St.8 denote thermodynamic stations.

At each compression stage, the outlet temperature is determined from the polytropic relation:

$$T_{out} = T_{in} \cdot \pi^{((n_k - 1)/n_k)} \tag{1}$$

where π is the stage pressure ratio and $n_k = 1.395$ is the polytropic index. The energy flux imparted to the air by each compressor stage is:

$$Q_{comp} = \dot{m}_{air} \cdot c_{a} \cdot (T_{out} - T_{in}) \tag{2}$$

In the combustion chamber, the total gas energy flux is:

$$Q_{gas} = Q_{air} + \xi \cdot Q_{fuel} \tag{3}$$

where $Q_{fuel} = (C_h \cdot Q_i)/3600$. The temperature rise across the combustion chamber is computed from the gas energy flux and the exhaust gas mass flow rate. For each turbine stage, the energy extracted by the gas is:

$$Q_{g,turb} = Q_{comp}/(\eta_T \cdot \eta_C) \tag{4}$$

and the corresponding temperature drop is:

$$\Delta T_{turb} = Q_{g,turb}/(\dot{m}_{gas} \cdot c_g) \tag{5}$$

The overall thermal efficiency of the gas turbine installation is evaluated as:

$$\eta_e = (Pe_{ITG} \cdot 3600)/(C_h \cdot Q_i) \tag{6}$$

The CFD simulations were conducted on a simplified single-stage rotor model representing the high-pressure turbine of a two-spool naval gas turbine. The rotor blades were modelled starting from a planar rectangular profile, subsequently flexed to introduce the required aerodynamic twist, and replicated using Circular Pattern to distribute 24 blades uniformly around the disc circumference. The blade shape was refined using the Revolved Cut function applied to a Spline-defined profile, achieving the characteristic cambered cross-section of an axial turbine blade, consistent with design practices described by Xu et al. (2018). The computational domain was defined as an internal flow region rotating with the rotor. Three operating regimes were investigated, with inlet boundary conditions of velocity, temperature, and pressure assigned as representative of the thermodynamic state at the high-pressure turbine inlet as determined by the energy flow calculations. For each regime, the simulation was run until convergence, defined as the stabilisation of total pressure values at both rotor inlet and outlet. Total pressure at inlet and outlet was recorded as the primary output parameter, and the relative pressure drop across the rotor was computed as the ratio of pressure differential to inlet pressure.

3. Results and discussions

This section presents the numerical results obtained from the thermodynamic energy flow calculation of the Rolls Royce gas turbine and from the CFD simulations of the high-pressure turbine rotor. Results are reported sequentially, following the methodology described in Section 2.

3.1. Energy Flow Calculation Results

The air, fuel, and exhaust gas mass flow rates are derived from the nominal fuel consumption rate and the air excess coefficient (Table 1). The air excess coefficient $\alpha = 1.64$ indicates that the combustion process uses 64% more air than the stoichiometric minimum, which is characteristic of gas turbines operating with lean premixed combustion to limit peak flame temperatures and associated thermal stresses on hot-section components (Fatsis, 2022). The fuel-to-air ratio by mass is 0.278/6.56 = 0.0424, which is significantly below the stoichiometric value of 0.0694 for diesel fuel, confirming the lean operating regime. The exhaust gas mass flow rate of 6.838 kg/s is the sum of the air and fuel mass flow rates and serves as the reference flow for all downstream turbine calculations.

Table 1. Mass flow rates at nominal operating conditions.

Parameter	Symbol	Value	Unit
Air mass flow rate	$\dot{m}_{air}$	6.56	kg/s
Fuel mass flow rate	$\dot{m}_{fuel}$	0.278	kg/s
Exhaust gas mass flow rate	$\dot{m}_{gas}$	6.838	kg/s

The thermodynamic parameters (Table 2) at all eight cycle stations reveal a temperature progression from 288.15 K at station 1 to 1,272.4 K at station 4, illustrating the combined effect of two-stage polytropic compression and combustion heat addition. The total temperature rise across the two compressor stages is 270.6 K, while the combustion chamber adds a further 713.7 K, bringing the gas to 1272.4 K at the high-pressure turbine inlet. The temperature drop across the three turbine stages totals 595.1 K, with the high-pressure turbine accounting for 230.9 K, the power turbine for 256.9 K, and the low-pressure turbine for 107.3 K. The exhaust temperature at station 7 of 677.3 K is substantially above ambient, indicating significant residual enthalpy in the exhaust stream. This represents an opportunity for waste heat recovery in a combined gas-and-steam configuration, a principle already demonstrated in commercial cruise ship propulsion (Budiyanto et al., 2024).

Table 2. Thermodynamic parameters at all cycle stations.

Station	Description	p (bar)	T (K)
0	Atmosphere	1.013	288.15
1	LPC inlet	1.013	288.15
2	LPC outlet / HPC inlet	2.543	374.0
3	HPC outlet / CC inlet	10.502	558.7
4	CC outlet / HPT inlet	~10.0	1272.4
5	HPT outlet / LPT inlet	~5.8	1041.5
6	LPT outlet / PT inlet	~2.8	934.3
7	PT outlet	~1.3	677.3
8	Exhaust to atmosphere	1.013	288.15

The energy fluxes at each component show that of the total fuel energy input of 11,861 kW, only 1,863.7 kW is carried by compressed air entering the combustion chamber, meaning that 84.6% of the thermal input comes directly from combustion. The fuel energy utilisation factor $\xi = 0.523$, Bălan (2016), reflects incomplete conversion of chemical energy to useful gas enthalpy, accounting for combustion losses and radiation. The compressor drive power of 2,272.8 kW represents 56.8% of the total shaft power generated by all three turbine stages, which is characteristic of open-cycle gas turbines without intercooling or recuperation (Campora, 2024). The power turbine output of 1,727.2 kW constitutes the net propulsive contribution.

Table 3. Energy fluxes at each gas turbine component.

Component	Parameter	Value (kW)
Low-pressure compressor (LPC)	$\dot{Q}_{1a}$ - energy added to air	591.3
High-pressure compressor (HPC)	$\dot{Q}_{2a}$ - energy added to air	1,272.4
Air entering combustion chamber	$\dot{Q}_{air}$	1,863.7
Combustion chamber	$\dot{Q}_{fuel}$ - fuel energy flux	11,861.0
Combustion chamber	$\dot{Q}_{gas}$ - total gas energy flux	8,067.0
HPT driving HPC	$\dot{Q}_{TCH}$ - gas energy extracted	1,892.3
LPT driving LPC	$\dot{Q}_{TCL}$ - gas energy extracted	879.4
Power turbine (PT)	$\dot{Q}_{TP}$ - gas energy extracted	2,106.0
Exhaust to atmosphere	$\dot{Q}_{ev}$ - heat rejected	3,189.5

The overall thermal efficiency of $\eta_e = 0.337$ is consistent with published values for two-spool open-cycle gas turbines of comparable compression ratio and turbine inlet temperature, which typically range between 0.28 and 0.38 (Fatsis, 2022; Campora, 2024). The Sankey-type energy distribution analysis reveals that the dominant loss mechanisms are the combustion chamber thermal losses, accounting for 39.4% of total fuel energy, and the exhaust heat rejection at 26.9%. The exhaust stream carries 3,189.5 kW of recoverable thermal energy at 677.3 K, identified as a primary target for waste heat recovery. In modern gas turbines with advanced annular combustors, fuel energy utilisation factors of 0.96–0.99 are achievable, which would significantly improve both cycle efficiency and exhaust temperature

(Niculescu et al., 2020). These findings are consistent with the energy balance methodology applied by Campora (2024) to the WR21 marine gas turbine and by Fatsis (2022) to wave-rotor-enhanced cycles.

Table 4. Overall performance indicators of the Rolls Royce gas turbine installation.

Parameter	Symbol	Value	Unit
Effective power output	Pe_{ITG}	4,000	kW
Compressor drive power	P_{antK}	2,272.8	kW
Net power turbine output	P_{TP}	1,727.2	kW
Specific fuel consumption	c_e	0.250	kg_{fuel}/kWh
Specific thermal energy	q_e	10,675.5	kJ/kWh
Overall thermal efficiency	η_e	0.337	-
Power turbine efficiency contribution	η_{eTP}	0.145	-

3.2. HP Turbine Rotor Geometry

The 3D model of the high-pressure turbine rotor was developed in SolidWorks and comprises nine individual components assembled into a complete rotor stage (Figure 1). The blade profile was defined using Spline curves, and each blade was flexed to introduce the required twist angle. The resulting geometry approximates the aerodynamic requirement of a constant-work axial turbine stage, in which the blade angle varies from root to tip to maintain uniform energy extraction across the blade height, consistent with standard design practice for high-pressure turbine rotors (Xu et al., 2018; GE Aerospace, 2024). The rotor geometry was intentionally simplified relative to a production rotor, omitting internal cooling passage networks, blade tip seals, and inter-stage stator vanes, in order to isolate the effect of rotational speed on the through-flow pressure distribution. This level of geometric fidelity is consistent with parametric CFD studies of simplified turbine stage models used for performance analysis in the literature (Xu et al., 2018).

3.3. CFD Simulation Results

At a rotational speed of 500 rad/s, with inlet conditions of v = 100 m/s, T = 1,250 K, and p = 1.80 MPa, the total pressure at the rotor inlet stabilised at 1.820 MPa and at the rotor outlet at 1.800 MPa, yielding a pressure drop of 0.020 MPa, corresponding to 1.10% of the inlet pressure. Convergence was achieved after approximately 50 iterations, as indicated by the stabilisation of both inlet and outlet total pressure curves. The low-pressure drop at this regime is consistent with the moderate centrifugal loading on the blades at reduced rotational speed, resulting in limited work extraction per unit mass of gas, as seen in Figure 3.

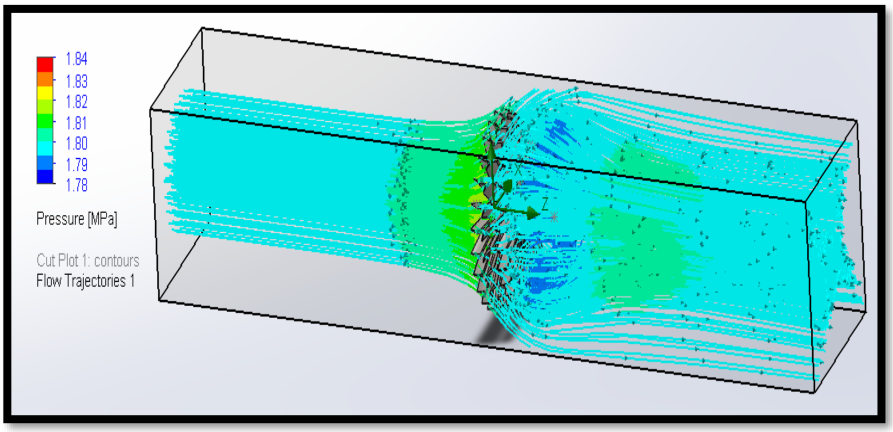

Figure 3. Total pressure distribution across the HP rotor at 500 rad/s - SolidWorks Flow Simulation result.

At 750 rad/s, with inlet conditions of v = 125 m/s, T = 1,350 K, and p = 2.15 MPa, the total pressure drop was 0.036 MPa, representing 1.64% of the inlet pressure — a 49% increase relative to the 500 rad/s regime despite only a 50% increase in rotational speed, as seen in Figure 4. This nonlinear relationship reflects the quadratic dependence of blade work on peripheral velocity, whereby doubling the angular velocity yields approximately four times the specific work, as described by Euler's turbomachinery equation (Xu et al., 2018).

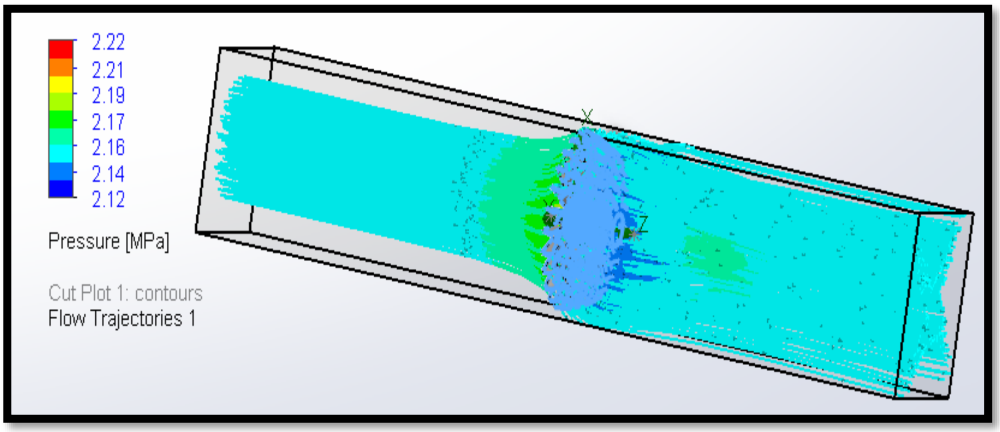

Figure 4. Total pressure distribution across the HP rotor at 750 rad/s - SolidWorks Flow Simulation result.

At 1,000 rad/s, with inlet conditions of v = 150 m/s, T = 1,400 K, and p = 2.50 MPa, the pressure drop reached 0.060 MPa, corresponding to 2.34% of the inlet pressure - the largest drop recorded across all three regimes, and three times the value at 500 rad/s. The increased inlet pressure and temperature reflect the higher enthalpy state expected at elevated operating speeds, consistent with stage loading theory (Fatsis, 2022). The pressure field at this regime is shown in Figure 5.

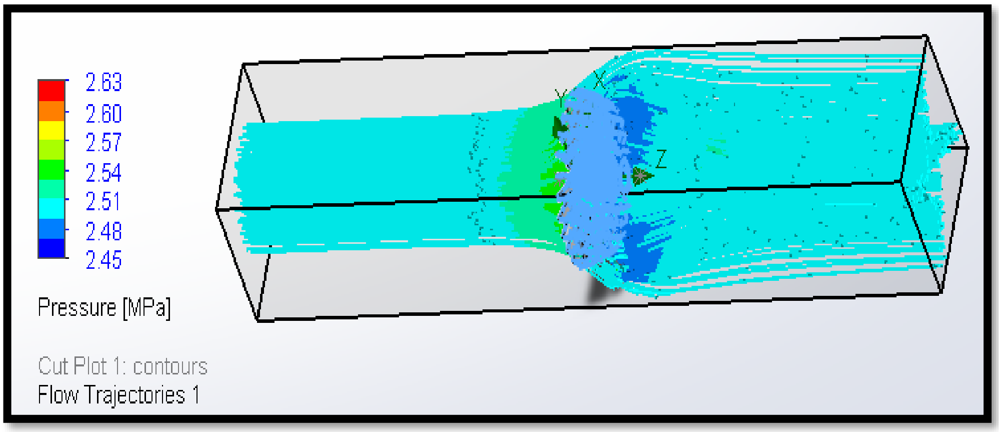

Figure 5. Total pressure distribution across the HP rotor at 1000 rad/s - SolidWorks Flow Simulation result.

A summary of the total pressure results across all three simulated regimes is presented in Table 5.

Table 5. Summary of CFD simulation results for the HP rotor across all speed regimes.

Regime	**ω (rad/s)**	**p_{in} (MPa)**	**p_{out} (MPa)**	**Δp (MPa)**	**$Δp/p_{in}$ (%)**
1	500	1.820	1.800	0.020	1.10
2	750	2.192	2.156	0.036	1.64
3	1,000	2.568	2.508	0.060	2.34

The pressure drop across the rotor increases monotonically with rotational speed, from 1.10% at 500 rad/s to 2.34% at 1,000 rad/s. The rate of increase is not perfectly linear: from the first to the second regime, the pressure drop increases by 0.016 MPa, while from the second to the third it increases by 0.024 MPa. This behaviour is consistent with the fundamental operating principle of axial turbine stages: at higher rotational speeds, the rotor blades perform greater work on the gas, resulting in a larger enthalpy drop and a larger pressure differential between inlet and outlet (Coraddu et al., 2016; Ma et al., 2023). The moderate absolute values of the pressure drop are attributable to the simplified single-passage geometry, which does not include upstream stator vanes or inter-stage flow effects. In a complete stage including nozzle guide vanes, total pressure drops of 15–25% would be expected for a high-loading turbine stage. The convergence behaviour observed across all three regimes confirms the numerical reliability of the SolidWorks Flow Simulation framework for parametric rotor studies at this level of geometric fidelity.

The fuel energy distribution across the gas turbine cycle is illustrated using a Sankey-type representation in Figure 6 and quantified in Table 6. Of the total fuel energy input of 11,861 kW, only 33.7% is converted into useful shaft power (4,000 kW). The remaining 66.3% is lost through two principal pathways: heat rejected to the atmosphere via the exhaust stream (3,189.5 kW, 26.9%) and thermal losses within the combustion chamber associated with incomplete energy utilisation (4,671.5 kW, 39.4%). This distribution is characteristic of simple open-cycle gas turbines without recuperation or intercooling, where the exhaust heat rejection and combustion inefficiency represent the dominant loss mechanisms. The compressor work of 2,272.8 kW, while not a thermodynamic loss per se, constitutes a significant internal energy recirculation that reduces the net propulsive output of the power turbine to 4,000 kW (effective shaft power).

Table 6. Fuel energy distribution across the gas turbine cycle.

Energy destination	Value (kW)	Share of $\dot{Q}_{fuel}$ (%)
Useful shaft power (Pe_{ITG})	4,000.0	33.7
Heat rejected to atmosphere ($\dot{Q}_{ev}$)	3,189.5	26.9
Combustion chamber losses ($1 - \xi$)	4,671.5	39.4
Total fuel energy input	11,861.0	100

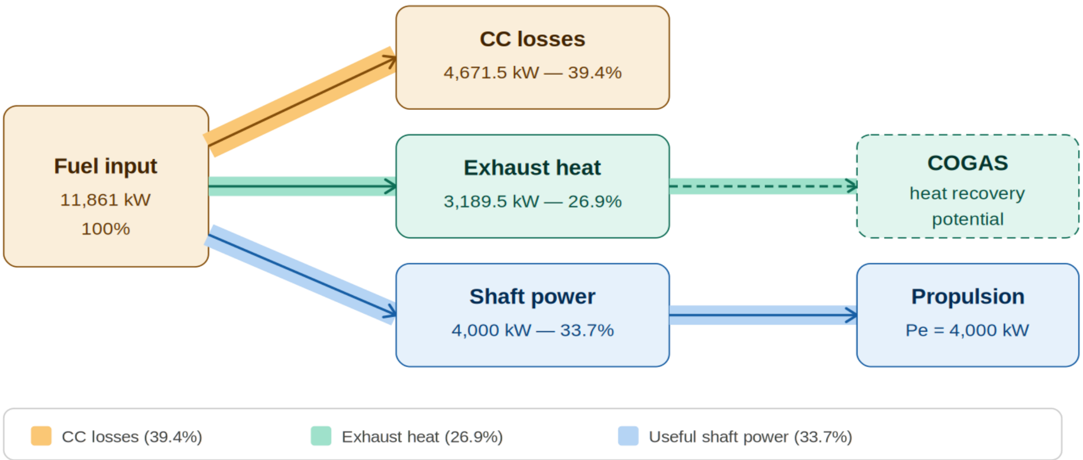

Figure 6. Sankey-type energy distribution diagram for the Rolls Royce gas turbine installation. Fuel input: 11,861 kW. Amber - combustion chamber thermal losses (39.4%); green - exhaust heat rejected to atmosphere (26.9%), with potential for COGAS recovery (dashed); blue - useful shaft power delivered to propulsion (33.7%).

4. Conclusions

This paper presented a combined analytical and numerical study of a naval gas turbine propulsion system, structured around two complementary contributions: a complete thermodynamic energy flow calculation for the Rolls Royce gas turbine, and a CFD parametric simulation of the high-pressure turbine rotor at three rotational speed regimes.

The novelty of this study resides in the simultaneous treatment of two aspects that are rarely addressed together in the open literature: the station-by-station thermodynamic characterisation of the full Rolls Royce gas turbine cycle, and the CFD-based pressure distribution analysis of a 3D rotor model, applied in the context of a concrete naval platform modernisation scenario. While previous studies have addressed either thermodynamic cycle modelling (Campora, 2024; Fatsis, 2022) or turbine rotor simulation (Xu et al., 2018) in isolation, the present work integrates both approaches within a single propulsion system study, providing a more complete basis for performance assessment. The Sankey-type energy distribution analysis, identifying the combustion chamber losses at 39.4% and exhaust heat rejection at 26.9% as the dominant inefficiency pathways, offers directly actionable information for propulsion system optimisation that is not typically reported for this class of naval gas turbine.

Several limitations of the present study should be acknowledged. First, the CFD simulations were performed on a geometrically simplified single-passage rotor model that omits nozzle guide vanes, blade cooling passages, tip clearance effects, and inter-stage flow interactions. As a consequence, the pressure drop values obtained represent conservative lower-bound estimates of the actual stage pressure ratio.

Second, the thermodynamic calculation relies on a uniform isentropic efficiency assumption for all compressor and turbine stages, which does not capture the variable stage loading and off-design performance characteristic of real two-spool machines. Third, the combustion chamber energy utilisation factor $\xi = 0.523$ is based on nominal documentation values and may not reflect the actual combustion efficiency under variable fuel-air ratio conditions (Bălan, 2016; Niculescu et al., 2020). These limitations can be progressively overcome through the adoption of higher-fidelity CFD models incorporating full-annulus stage geometries, variable efficiency maps derived from experimental data, and detailed combustion modelling using reactive flow solvers.

The results of this study have direct practical relevance for the modernisation of naval propulsion systems. The thermodynamic energy balance demonstrates that the exhaust stream carries 3,189.5 kW of recoverable thermal energy at 677.3 K, representing a strong case for the adoption of a COGAS configuration that could raise overall plant efficiency from 33.7% toward 40–42% (Budiyanto et al., 2024). The CFD rotor simulation results provide a quantitative basis for blade geometry optimisation studies, particularly with respect to twist angle distribution and leading-edge profile, which directly influence stage pressure ratio and energy extraction efficiency. The proposed replacement of the original Tyne/Olympus arrangement with the GE LM2500 and Pratt & Whitney ST40M turbines reduces cruise engine mass by 59% and envelope volume by approximately 40%, yielding significant benefits in terms of payload capacity, acoustic signature reduction and maintenance accessibility (GE Aerospace, 2024; Niculescu et al., 2020). These findings are applicable to any naval platform of similar displacement and speed profile currently operating with first-generation gas turbine propulsion.

Future work should address the extension of the CFD analysis to a complete turbine stage including nozzle guide vanes, the incorporation of blade cooling passage effects, and the application of digital twin methodology to real-time performance monitoring of the propulsion installation (Ma et al., 2023; Coraddu et al., 2016). Performance-based health monitoring and prognostics frameworks, as reviewed by Tahan et al. (2017), represent a natural complement to the simulation methodology presented here, enabling condition-based maintenance of naval gas turbine installations. The integration of waste heat recovery into the energy balance, through a COGAS arrangement, represents a further avenue for improving the overall plant efficiency.

Author contributions:

- Conceptualization: V.O.N. and P.A.
- Methodology: V.O.N. and M.D.
- Investigation: V.O.N. and C.D.
- Writing original draft: V.O.N. and S.I.C.
- Writing review and editing: V.O.N. and M.D.
- Supervision: V.O.N.

Funding: this research received no external funding

Conflict of interest: The Authors declare no Conflict of interest.

References

1. Bălan, G. (2016). Turbine cu gaze — Elemente de teorie și aplicații navale. Editura Academiei Navale "Mircea cel Bătrân".
2. Bob-Manuel, K. D. H., & Okim, B. O. (2018). Optimising technique in matching combined diesel engine or gas turbine (CODOG) propulsion system to hull and propeller of a frigate. Proceedings of the International Naval Engineering Conference and Exhibition (INEC). https://doi.org/10.24868/issn.2515-818x.2018.035

3. Budiyanto, M. A., Nasruddin, N., Sari, R. M., & Yulianto, M. (2024). Techno-economic analysis of combined gas and steam propulsion system of liquefied natural gas carrier. Energies, 17(6), 1415. https://doi.org/10.3390/en17061415
4. Campora, U. (2024). WR21 marine gas turbine thermodynamic simulator for ship propulsion studies. International Journal of Frontiers in Engineering and Technology Research, 6(1), 001–015. https://doi.org/10.53294/ijfetr.2024.6.1.0023
5. Coraddu, A., Oneto, L., Ghio, A., Savio, S., Anguita, D., & Figari, M. (2016). Machine learning approaches for improving condition-based maintenance of naval propulsion plants. Proceedings of the Institution of Mechanical Engineers Part M: Journal of Engineering for the Maritime Environment, 230(1), 136–153. https://doi.org/10.1177/1475090214540874
6. Dassault Systèmes. (2023). SolidWorks — The solution for 3D CAD, design and product development. https://www.solidworks.com/
7. Fatsis, A. (2022). Gas turbine performance enhancement for naval ship propulsion using wave rotors. Journal of Marine Engineering and Technology, 21(5), 297–309. https://doi.org/10.1080/20464177.2021.1933697
8. Friedman, N. (2006). The Naval Institute Guide to World Naval Weapon Systems. Naval Institute Press.
9. GE Aerospace. (2024). LM2500 Gas Turbine Engine. https://www.geaerospace.com/military-defense/engines/lm2500
10. Ghose, J. P., & Gokarn, R. (2004). Basic Ship Propulsion. McGraw-Hill Education.
11. Homišin, J., Kaššay, P., Urbanský, M., Puškár, M., Grega, R., & Krajňák, J. (2020). Electronic constant twist angle control system suitable for torsional vibration tuning of propulsion systems. Journal of Marine Science and Engineering, 8(9), 721. https://doi.org/10.3390/JMSE8090721
12. Ma, Y., Zhu, X., Lu, J., Yang, P., & Sun, J. (2023). Construction of data-driven performance digital twin for a real-world gas turbine anomaly detection considering uncertainty. Sensors, 23(15), 6660. https://doi.org/10.3390/s23156660
13. Niculescu, F., Borzea, C., & Vasile, M. L. (2020). Marine gas turbine for efficient ship propulsion. Scientific Bulletin of Naval Academy, 23(2), 214–221.
14. Ren, H., Ding, Y., & Sui, C. (2019). Influence of EEDI on ship-engine-propeller matching. Journal of Marine Science and Engineering, 7(12), 425. https://doi.org/10.3390/JMSE7120425
15. Sahraoui, M. A., Rahmoune, C., Damou, A., Gougam, F., & Afia, A. (2024). Advancing condition-based maintenance of naval propulsion systems with ensemble learning techniques. Advances in Mechanical Engineering, 16. https://doi.org/10.1177/16878132241298373
16. Siemietkowski, J. S. (1970). Maintenance of marine gas turbine engines. Proceedings of the ASME Gas Turbine Conference, GT1970-51. https://doi.org/10.1115/70-GT-51
17. Sui, C., de Vos, P., Stapersma, D., Visser, K., & Ding, Y. (2020). Fuel consumption and emissions of ocean-going cargo ship with hybrid propulsion and different fuels over voyage. Journal of Marine Science and Engineering, 8(8), 588. https://doi.org/10.3390/JMSE8080588
18. Tahan, M., Tsoutsanis, E., Muhammad, M., & Karim, Z. A. A. (2017). Performance-based health monitoring, diagnostics and prognostics for condition-based maintenance of gas turbines: A review. Applied Energy, 198, 122–144. https://doi.org/10.1016/j.apenergy.2017.04.048
19. Xu, Z., Wen, X., & Zhao, N. (2018). A novel COGAG propulsion system for marine ships. Proceedings of the ASME Turbo Expo, GT2018-75908. https://doi.org/10.1115/GT2018-75908
20. Zhu, Y., Tan, H., & Ying, Y. (2021). Recent advances in CFD simulations of gas turbine flows: A review. Progress in Aerospace Sciences, 126, 100754. https://doi.org/10.1016/j.paerosci.2021.100754